# A Power Sensor Tag With Interference Reduction for Electricity Monitoring of Two-Wire Household Appliances

Yung-Chang Chen, Wei-Hung Hsu, Shih-Hsien Cheng, and Yu Ting Cheng, *Senior Member, IEEE*

***Abstract*—This paper demonstrates a flexible nonintrusive power sensor tag with an interference reduction scheme for accurate electricity monitoring of the household appliances using typical SPT-2 18 AWG zip-cord power lines. Both current and voltage sensors with the design of a 50-turn inductive coil and two capacitive electrodes, respectively, in an area of $1.3 \times 1$ cm$^2$ are fabricated on a 100-$\mu$m-thick flexible polyethylene terephthalate substrate as a sensor tag. The tag exhibits a sensitivity of 271.6 mV/A and 0.38 mV/V via active low-pass filter circuits for the current and voltage detection. A compensation circuit inputted with the signals of the voltage sensor is applied for the interference reduction of the current sensor electrically coupled with the power cord so that the current sensor can achieve over a 40-dB signal-to-noise ratio for measuring the loaded current of 1 A, 60 Hz on the power line.**

***Index Terms*—Flexible sensor and nonintrusive, household electricity monitoring, power sensor tag.**

## I. Introduction

As GLOBAL warming effects resulting from $CO_2$ emission become more severe, most of the countries in the world are dedicated to the improvement of the energy efficiency. One of the important energy-reservation strategies is to construct advanced metering infrastructure for the promotion of time-based pricing to reduce peak load, increase the efficiency of energy use, and improve the quality of electricity service. With the concept of "Smart Grids" [1], the electricity monitoring systems possessing the demand response (DR) capability have been reported to be a cost-effective apparatus to well manage electricity usage in residential areas for energy reservation [2].

For the pervasive deployment of the DR monitoring system, robust, low cost, easy to use, and small form factor are the key features of the power sensing system for monitoring 50/60-Hz household electricity. A power monitoring system comprises current and voltage sensors. The current sensors have been widely utilized for industrial appliance monitoring applications and are generally designed with the detection of magnetic field generated by the electric current flowing through power cords. Such a current sensor is contactless, very suitable for the pervasive power detection of household appliances owing to nondestructive and easy-implementation characteristics. These current sensors include the Rogowski coil, current transformer (CT), fluxgate, Hall-effect sensor, magnetoimpedance sensor, and so on [3]–[5]. The Rogowski coil is designed with a spiral air-core coil winding around a source conductor for current measurement based on Faraday's law of induction. Without being implemented with a ferromagnetic core, the coil sensor can exhibit highly linear sensitivity and wide operation bandwidth, and it is capable of measuring large current without saturation [6], [7]. For low current measurement, the Rogowski coil must be integrated with a high performance amplifier. For example, Rigoni *et al.* presented a Rogowski coil with 3626 loops connected to a low noise active filter with gains of thousands for milliamperes of current detection [8]. Similar to the geometry of the Rogowski coil, CT is designed with the coil structure composed of a primary coil, a secondary coil, and an embedded bulk ferromagnetic ring core [9]. It detects the current by encircling the source conductor with the sensor coils. However, the saturation and hysteresis effects on the magnetization resulting in detection error should be considered while the source current contains a dc component or is loaded with the ac current in a high-frequency regime. Periodical calibration is required for the CT to keep the accuracy in measurement [3]. Since the Rogowski coil and CT can only detect the current flowing through a single current-carrying conductor, they are not useful in the electricity monitoring of household appliances usually accompanied with a power cable containing two or three power wires.

Fluxgate current sensors have two coils, which are driving and sensing coils winding around a ferromagnetic core, respectively, for measuring dc or low-frequency magnetic fields. Although the resolution can be as low as 10 pT, the inevitable large size and intricate reading circuit of the sensor to accomplish precise measurement make the sensor itself not practical for being distributed over household appliances. Liakopoulos and Ahn presented a microfluxgate magnetic sensor fabricated using UV-LIGA process for achieving a sensing resolution of 10 nT in a volume less than 1 cm$^3$ [10]. Rovati and Cattini demonstrated a simple and sensitive readout circuit for planar fluxgate sensors whose sensitivity can be easily set from 13.3

Manuscript received April 25, 2013; accepted May 11, 2013. Date of publication June 4, 2013; date of current version September 19, 2013. This work was supported in part by the National Science Council (NSC) 101-2220-E-009-007 project and in part by the Ministry of Education in Taiwan under the Aim for the Top University (ATU) Program.

Y.-C. Chen, W.-H. Hsu, and Y. T. Cheng are with the Department of Electronics Engineering and Institute of Electronics, National Chiao Tung University, Hsinchu 30010, Taiwan (e-mail: ycchen.ee97g@g2.nctu.edu.tw; wayhome23.ee99g@g2.nctu.edu.tw; ytcheng@mail.nctu.edu.tw).

S.-H. Cheng is with the Institute of Electrical Control Engineering, National Chiao Tung University, Hsinchu 30010, Taiwan, and also with the Green Energy and Environment Research Laboratories, Industrial Technology Research Institute, Chutung 31040, Taiwan (e-mail: ShrShianJeng@itri.org.tw).

Color versions of one or more of the figures in this paper are available online at http://ieeexplore.ieee.org.

Digital Object Identifier 10.1109/TIE.2013.2266089

to 104.9 mV/$\mu$T [11]. Nevertheless, large driving current up to 300 mA, i.e., $\sim$100-mW power consumption, or 10-kHz 600-mA current injecting into the excitation coil is required to ensure the saturation of the core for field sensing. The SQUID magnetometer is another type of fluxgate sensor and also one of the most sensitive vector magnetometers in the world. However, it must be operated at very low temperature. Thus, the necessity of either large power consumption or low temperature operational environment will hinder these sensors for long-term operation, particularly in residential applications.

Magnetoresistivity effect can be utilized for magnetic field detection. The magnetic field-dependent resistance change of conductive materials, such as anisotropic magnetoresistance, giant magnetoresistance (GMR), or tunnel magnetoresistance films, mainly resulted from the spin-orbital coupling effect [12]. The precise thickness and composition of the multilayered magnetic structures to ensure the magnetized orientation may increase the fabrication cost. The phenomenon of magnetoresistivity change has also been observed in magnetic Permalloy whose resistivity change is caused by the influence of the Lorenz force on the motion of carriers. Although the alloy can be electroplated and utilized as a low-cost magnetic sensor material, nonlinear behavior and large thermal dependence would limit the sensor accuracy.

Hall-effect sensors have been widely applied for dc and ac magnetic field measurement. Via a constant current flowing through a thin conductive layer applied with an external magnetic field, a voltage generated in the perpendicular direction can be utilized as an indicator to evaluate the field strength. In fact, the sensor can be miniaturized using CMOS process to fully integrate a readout circuit for better performance and lower manufacture cost. Recently, Frick *et al.* presented a silicon Hall current sensor with a differential readout circuit that can detect a 50-Hz current with 0.5% accuracy in the range of 250 mA–5 A corresponding to a magnetic field of several milliteslas [13]. Nevertheless, while the household appliance is operated, the induced magnetic field around its PVC-insulated power cable is about an order of magnitude smaller than a millitesla that is almost equal to the offset voltage of the CMOS Hall-effect device, i.e., the misalignment voltage at a zero magnetic field. The Hall sensor therefore requires a delicate compensation circuitry for the current detection of household appliances. Although the Hall sensor with higher magnetic sensitivity, lower equivalent magnetic offset, and noise can be achieved by integrating a magnetic flux concentrator that guides the magnetic field in parallel with the chip surface to enhance the detected signal, the concentrator can be useful unless the sensor is not placed near any single wire in the zip cord, i.e., two-wire power line.

On the other hand, contactless voltage sensors are generally designed with the electrical coupling mechanism where sensor electrodes are utilized to collect the charges like a capacitor and connected to a readout circuit. These voltage sensors include the electric-field mill, electro-optical voltage transducer, FET- or varactor-based voltage sensors, etc. [16]–[19]. Wijeweera *et al.* presented a micromachined electric-field mill with a moving shutter that can detect both dc and ac fields [16]. The sensitivity of the mill depends on the mechanical performance of the shutter requiring a reliable vacuum package for accurate sensing and long-term operation. Noras presented a solid-state electric-field sensor based on variable capacitances capable of detecting 50/60-Hz voltages [19]. The varactors must be driven with a 1-MHz 10-V signal that requires a complex high voltage circuitry, while they are miniaturized and operated with the button cell battery for household electricity monitoring applications. Although the electro-optical sensor can provide accurate voltage sensing owing to its high immunity to electromagnetic interference, it is usually accompanied by a large, complicated, and expensive signal analyzing system that will make itself impractical for household applications. Meanwhile, few research works have been presented regarding the electricity monitoring system combining voltage and current sensors together. Kubo *et al.* showed a voltage/current sensor designed with two air coils and two electrodes for detecting the power transmission along a single power line applied with a kilovolt order of power which has been widely used in industrial manufactories [20]. Rowe *et al.* presented a nonintrusive load monitoring system by collecting the electromagnetic field generated from a 12 AWG wire using a FET-based electric-field sensor and a coil-based magnetic sensor via a readout circuit [18]. However, these sensing systems are not practical for the proposed power monitoring purpose because either most of the household appliances are equipped with the power input port using a two-wire line or the requirement of the millihertz-order inductor and 5-cm antenna power makes the sensor too large to be pervasively used for household appliances.

Basically, the two-wire power line contains two electric currents flowing in opposite directions, so the magnetic field around each single wire is quite small. The maximum field in the power line is perpendicular to the junction of the two wires. Leland *et al.* presented a microelectromechanical-systems-typed ac current sensor using a piezoelectric cantilever with a magnet mounted and placed on the top center of the two-wire power cable to get the largest sensitivity which is 0.1–1.1 mV/A [14], [15]. In order to realize small form factor, reliable, accurate, and ubiquitous current and voltage detection, we previously demonstrated a nonintrusive, low-cost, and reliable sensor tag closely fitted with the power cords of household appliances for current and voltage detection [21]. Instead of using a micromechanical structure to detect the maximum magnetic field, a planar spiral inductive coil is fabricated on a flexible substrate to sense the current in the two-wire power line of household appliances based on the detection of magnetic flux change. Meanwhile, by taking the advantage of good proximity provided by the flexible tag, capacitive electrodes are also devised on the same tag for voltage sensing.

Nevertheless, the current sensor still suffered from an electrical interference problem that resulted from the electric-field coupling of the load on the power cord. Because the proposed power sensor tag can exhibit better design and process integration with the existing CMOS technology and has revealed an alternative low-cost and pervasive current-sensing solution, the detail design, fabrication, characterization, and practice of the tag with an interference reduction scheme will be developed and depicted in this paper for advancing electricity monitoring systems for widespread use.

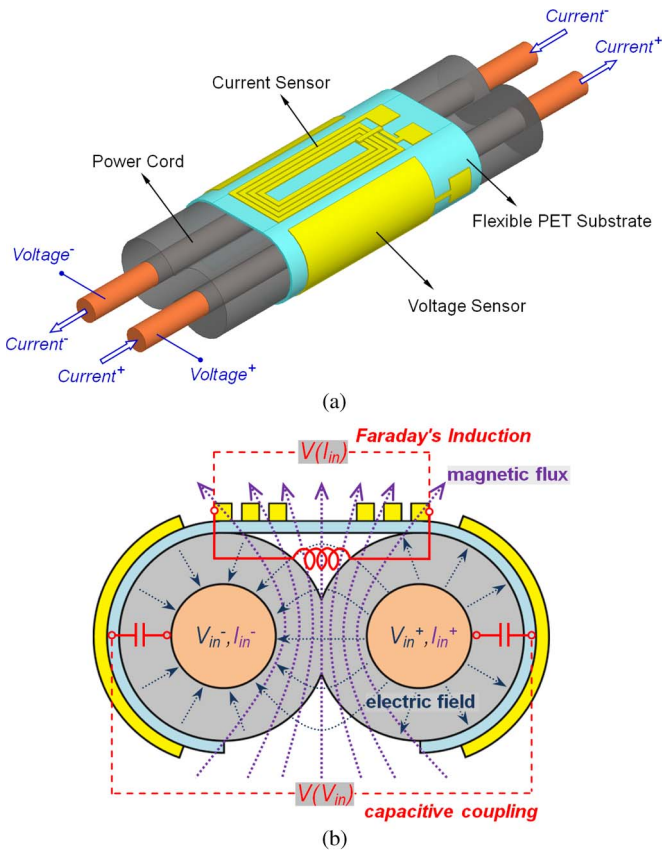


Fig. 1. (a) Scheme of the flexible nonintrusive power sensor tag with good proximity. (b) Cross-sectional view illustrating the sensing principle of the current sensor and voltage sensor [21].

## II. Design and Fabrication of Power Sensor

Fig. 1 shows the proposed power sensor tag designed for monitoring the electricity of household zip-cord power lines with the sensing principles addressed as follows.

The power sensor can be divided into two subcomponents: One is for current sensing, and the other is for voltage detection. Basically, the current sensor is an inductive coil operated by Faraday's law of induction. The voltage sensor comprises two pieces of metal pads working with the capacitive coupling mechanism. Since the magnetic and electric fields generated by the power source have $r^{-1}$ and $r^{-2}$ dependence, respectively, where $r$ is the distance from the sensing elements to the source, the proximity is the key to realize the high sensitivity of the nonintrusive sensors.

### A. Operational Principle of Current Sensor

According to the simulation of the magnetic field generated around a standard SPT-2 18 AWG power cord with a 1-A current input as shown in Fig. 2, the largest time-variant magnetic field will exist on the top or bottom sides of the central area of the two-wire cord. Therefore, an inductive coil tag can be used as the current sensor with the largest output voltage signal generated by the electric current flowing through the power cord, while it is closely attached to the power cord on the designated location. According to the Biot–Savart law, the

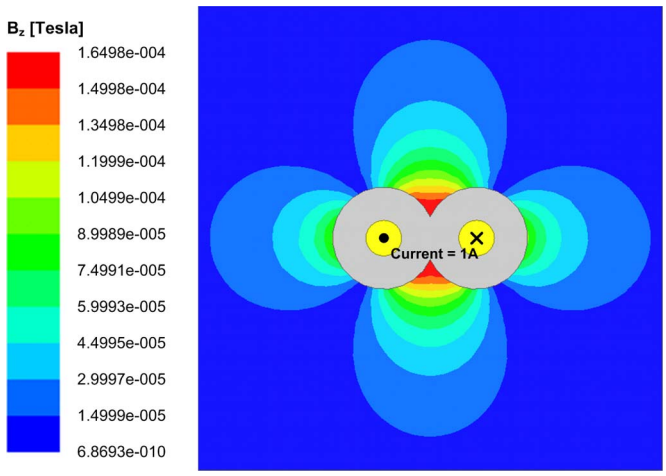


Fig. 2. Simulated magnitude of vertical component of the magnetic flux around a standard SPT-2 18 AWG power cord with 1-A current input.

magnetic flux density generated from a single current-carrying power cord is derived as follows [21], [22]:

$$\vec{B} = \frac{\mu_0 I \cos \omega t}{2\pi r} \hat{a}_\phi \tag{1}$$

where $B$ is the magnetic flux density, $I$ is the current inside the cord, $\omega$ is the angular frequency of current, and $r$ is the distance from the source to a point in space. Thus, in accordance with Faraday's law of induction, the induced voltage of the open-loop current-sensing coil, which is proportional to the magnetic flux change resulting from the time-variant current flowing through the power cord, can be further calculated as follows:

$$V_{\text{in}} = -\sum_{n=1}^{N} \frac{d\Phi_n}{dt} = -\sum_{n=1}^{N} \frac{d}{dt} \oint \frac{\mu_0 \cos \omega t}{\pi r} I \hat{a}_\phi \cdot d\hat{A}_n \tag{2}$$

where $V_{\text{in}}$ is the induced voltage of the coil, $N$ is the total number of the coil, $\Phi_n$ is the integral of the vertical component of magnetic flux passing through the $n_{\text{th}}$ turn area, and $A_n$ is the area of the $n_{\text{th}}$ turn of the coil. The detail analysis has been developed in the previous work [23]. By considering the dimension of the power cord, the thickness of the flexible substrate, the linewidth, spacing, turns of the sensing coil, etc., the sensitivity can be estimated. In this paper, the sensing coil is 50 turns designed with 21 $\mu$m in linewidth and 21 $\mu$m in spacing in an area of $10 \times 5$ mm$^2$.

### B. Operational Principle of Voltage Sensor

Fig. 3 shows the distribution of the electric field in a two-wire household power cord, where the neutral and fire lines applied with 0 and 115 V are located on the left and right sides of the cord, respectively. The result indicates that the electric field normal to the half circle interface on the right-hand side of the fire line is the best location with a sensing electrode that can exhibit the densest electrical flux, i.e., largest induced charge density, than that in any other location surrounding the power cord. Therefore, once the proposed voltage sensor comprising two electrodes pinches a power cord to sense a sinusoidal

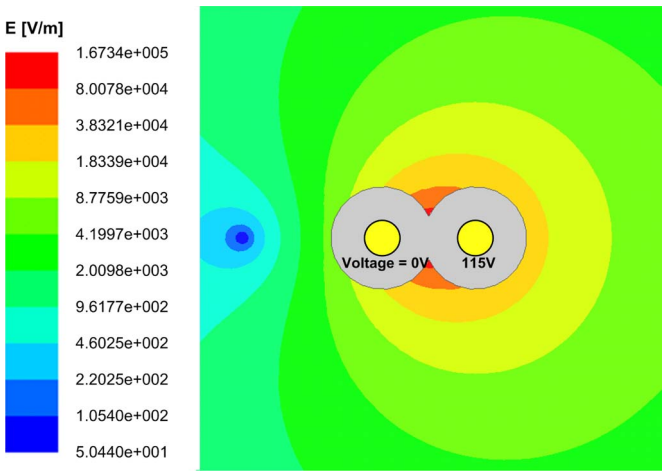


Fig. 3. Simulated electric field around the power cord with 0 V/115 V voltage applied on left/right line, respectively.

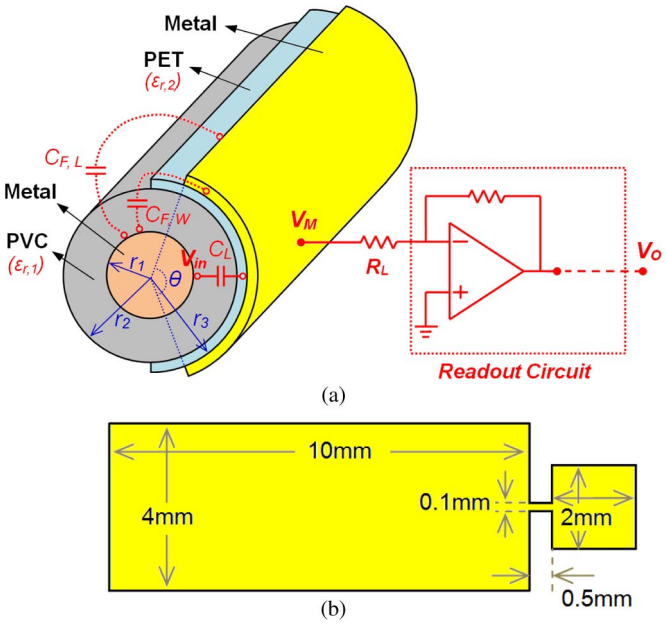


Fig. 4. Illustration of the (a) capacitances between the sensing electrode and the inner conductor of the power cord, including the cylindrical capacitance part and fringing capacitance part at each edge, and (b) dimensions of the sensing electrode.

electric field in the power cord, an ac current can be induced between the electrode and the inner conductor of the fire line while a current flow loop is established as shown in Fig. 4

$$i_C = C\frac{dV_c}{dt} \tag{3}$$

$$V_M = i_C R_L \tag{4}$$

where $C$ and $V_c$ are the capacitance and the voltage difference between the electrode and the inner conductor of the fire line, respectively. The induced current is equal to the multiple of the time derivative of the induced voltage and the capacitance proportional to the electrode area. The output voltage will depend on the total resistance of the connected circuit loop. To determine the characteristics of the voltage sensor, the capacitance between the cylindrical electrode and the inner conductor of the fire line, as shown in Fig. 4(a), can be estimated as follows:

$$C_L = \left[\sum_{n=1}^{N} \frac{\ln(r_{n+1}/r_n)}{\varepsilon_{r,n}\varepsilon_0\theta}\right]^{-1} \tag{5}$$

where $C_L$ is the partial coaxial capacitance per unit length, $r_n$ is the radius from the fire line center to the interface of the $n_{\text{th}}$ dielectric, i.e., PVC and polyethylene terephthalate (PET), $\varepsilon_{r,n}$ is the relative permittivity of the $n_{\text{th}}$ dielectric, $\varepsilon_0$ is the vacuum permittivity, and $\theta$ is the angle that the sensing electrode covered. It is noted that the fringing effect must be considered in this case since the ratio of the perimeter to the area in the sensing electrode cannot be neglected in the micrometer regime and there is no analytical model regarding the fringing capacitance of a finite concentric cylinder. Thus, in this work, an alternative method is employed to estimate the fringing capacitance by treating the capacitor as a parallel-plate capacitor as follows [24]:

$$C_F \cong \varepsilon_{r,1}\varepsilon_0 \frac{w}{h}\left[\frac{h}{\pi w} + \frac{h}{\pi w}\left(\frac{2\pi w}{h}\right)\right] \tag{6}$$

where $C_F$ is the fringing capacitance part per unit length, $w$ is the width of the sensing electrode, and $h$ is the gap distance between the electrode and the inner conductor surface. While the voltage induced on the sensing electrode, $V_1$, that is connected to a resistance load is much smaller than the voltage on the inner conductor of the fire line, $V_{\text{in}}$, the ac current in (3) can be derived as follows:

$$i_C = C\frac{dV_c}{dt} = C\frac{d(V_{\text{in}} - V_1)}{dt} \approx C\frac{dV_{\text{in}}}{dt} \quad \text{while} \quad V_{\text{in}} \gg V_1. \tag{7}$$

The output voltage can be therefore estimated by introducing the current $i_c$ to the readout circuit. In this case, the dimension of the sensing electrode is shown in Fig. 4(b). Moreover, the purpose of the voltage sensor is used not only for measuring the electricity voltage of the power cord but also for eliminating the interference noise of the current sensor that will be discussed later.

### C. Device Fabrication

Previously, we developed a flexible fabrication technology to assemble CMOS chips onto a SU-8 substrate [25]. Since the proximity is critical to the sensor performance, flexibility for close contact is a required design feature in the proposed sensor, and it can be realized by the developed technology to fabricate inductive coil and sensing electrodes on a flexible substrate simultaneously. In this paper, a flexible PET substrate instead of SU-8 glued to a silicon wafer is utilized for the flexible power sensor fabrication. The PET can have less residual stress and the same capability as SU-8 for flip-chip bonding with CMOS chips at a temperature below 250 °C at wafer level [26]. In addition, the PET is transparent and mechanically strong and has good resistance to moisture and chemicals. It is also inexpensive and can be easily acquired.

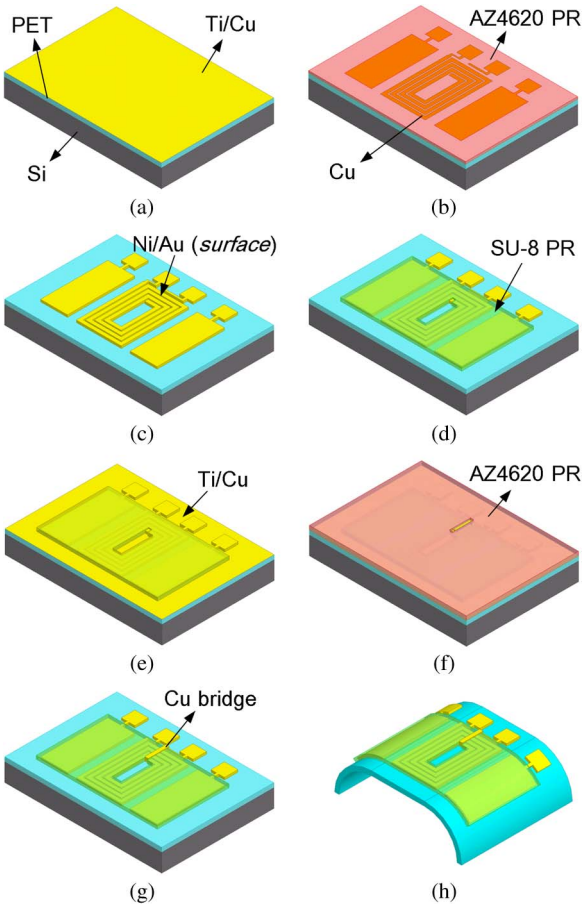


Fig. 5. Schematic process flow of the sensor tag fabrication (die level).

The fabrication process has been introduced previously as shown in Fig. 5 [21]. The whole process includes the following: 1) PET substrate preparation; 2) Ti/Cu (30 nm/90 nm) adhesion seed layer deposition; 3) inductor and capacitive electrode fabrication; and 4) sensor tag realization. It begins with the PET substrate, i.e., a 100-$\mu$m-thick A4 size slide, cutting to form a circular PET film which is glued onto a 4-in silicon handling wafer. The wafer is then sputtered with a layer of Ti/Cu (30 nm/90 nm) as an adhesion/seed layer [see Fig. 5(a)]. The inductive coil area of the current sensor and the electrodes area of the voltage sensor on the wafer are defined by AZ4620 photoresist using the conventional photolithography technique and then electroplated with a 2-$\mu$m-thick Cu coil and capacitor electrodes [see Fig. 5(b)]. After the removal of the AZ4620 photoresist by acetone and the Ti/Cu seed/adhesion layer by buffered HF and Cu etchant, respectively, the Cu surface is electroless plated with a thin Ni/Au layer for protecting the coil and electrodes from oxidation and corrosion [see Fig. 5(c)]. The metal patterns are covered with a 2-$\mu$m-thick SU-8 layer left with an opening via hole for air-bridging connection by photolithography [see Fig. 5(d)]. Another Ti/Cu adhesion/seed layer is sputtered and covered with a photopatterned AZ4620 photoresist as the mold for electroplating Cu bridge [see Fig. 5(e)]. After electroplating Cu [see Fig. 5(f)], the AZ4620 photoresist and Ti/Cu layer are removed using acetone and buffered HF and Cu etchant, respectively. [see Fig. 5(g)]. After detaching the PET substrate from the Si handling wafer, the sensor tag is accomplished by cutting the whole PET into pieces of the tags [see Fig. 5(h)]. Fig. 6 shows as-fabricated sensors on the PET substrate, and the inset shows good substrate flexibility in the sensor tag, which can be closely attached to the SPT-2 18 AWG power cord.

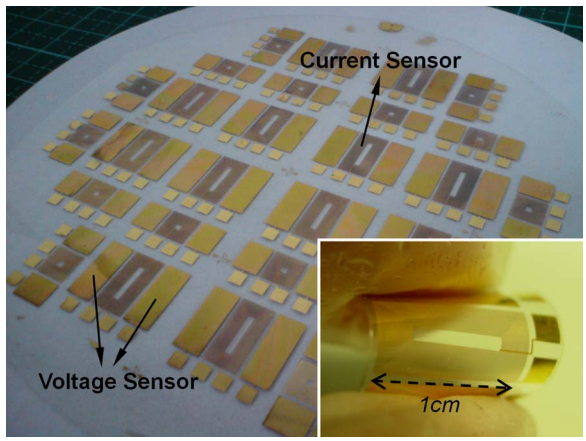


Fig. 6. As-fabricated sensors on a PET substrate. The insets shows good flexibility of the sensor tag closely stuck onto the tested standard SPT-2 18 AWG power cord.

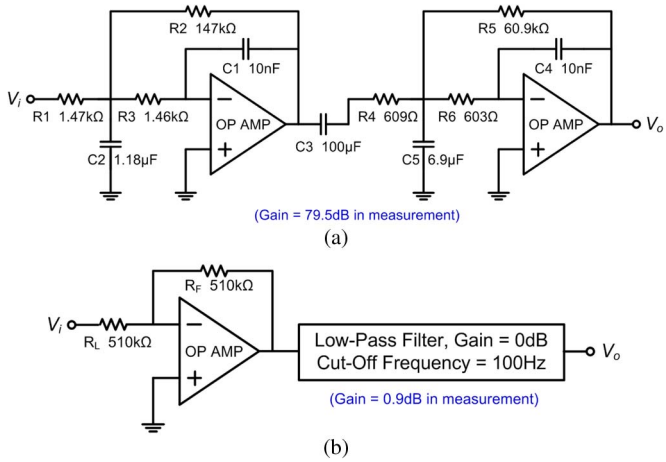


Fig. 7. (a) Active filter circuit with 80-dB 100-Hz cutoff frequency designed by TI FilterPro for the current sensor and (b) filter circuit designed for the voltage sensor with 0-dB 100-Hz cutoff frequency. The inverter is connected to the voltage sensor for providing a current path to virtual ground.

## III. Results and Discussion

### A. Device Characterization

The current and voltage sensors are connected to a fourth-order Butterworth low-pass filter functioning as a low-pass active filter to characterize the induced voltage from the coil and electrodes, respectively. The active low-pass filter circuit shown in Fig. 7(a) is designed with an 80-dB gain (79.5 dB in measurement) and a 100-Hz cutoff frequency by Texas Instruments FilterProTM software [27] for the current sensor. Another active filter circuit designed with a 0-dB gain (0.9 dB in measurement) and a 100-Hz cutoff frequency is used for the voltage sensor as shown in Fig. 7(b). Prior to the filter, the voltage sensor is connected to an inverter to provide a current path directly

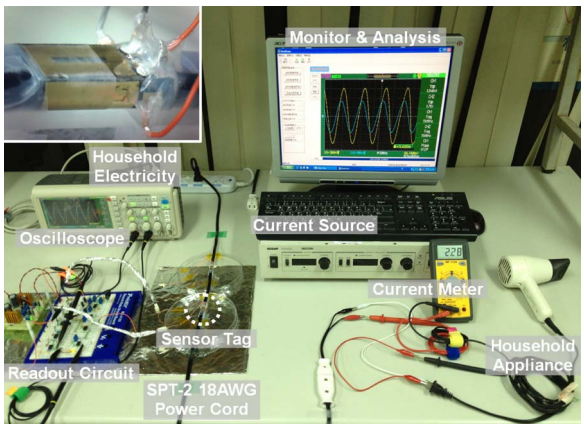


Fig. 8. Measurement setup including a current source for the characterization of the sensor tag and household electricity supply to verify the sensor tag.

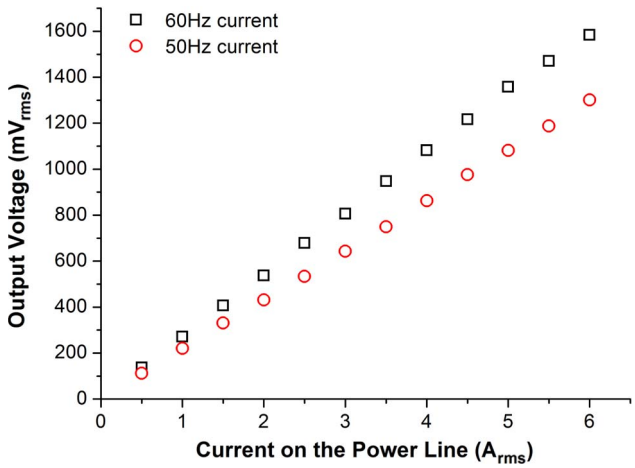


Fig. 9. Measured output voltage of the current sensor versus different input current at 50/60 Hz in the tested power line.

to the virtual ground that makes the measured sensing output solely depend on the resistive load. Fig. 8 shows the experimental setup. The current and voltage sensors are characterized respectively by monitoring the power input in a SPT-2 18 AWG power cord. The cord is loaded with a 1-A 50/60-Hz electric current supplied by the current source (ELGAR CW801M) in a short-loaded state and connected with the household 115-V 60-Hz power outlet in an open-loaded state, respectively, for the current and voltage sensor characterization.

Fig. 9 shows the output signal of the current sensor versus different input current flowing through the power cord at 50/60 Hz, and the correlation is linear as predicted in (2). Fig. 10 shows the output signal of the voltage sensor with different resistance loads versus the different input voltage applied on the power cord at 60 Hz. While the loads $R_L$ and $R_F$ referred to in Fig. 7(b) are modified from 510 kΩ to 300 or 755 kΩ, the output signals can be scaled by multiplying the ratio of the present and the former resistance based on (4). Fig. 10 also shows that the calculated output signal by substituting the reasonable dielectric constants, which are 5.4 for PVC and 3.4 for PET, to (3)–(7) can fit the measured results well. With the design of a 50-turn coil combined with two

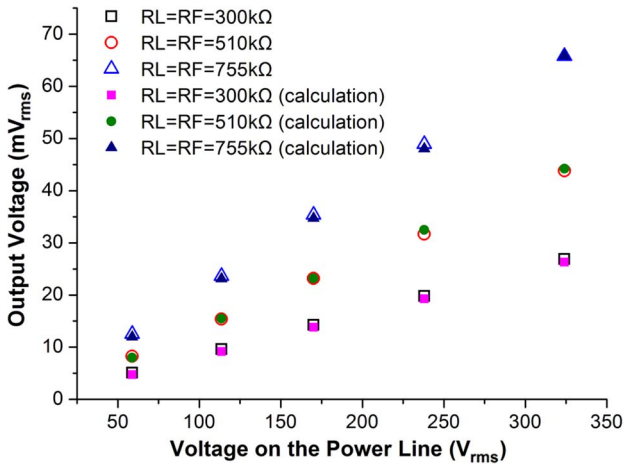


Fig. 10. Measured sensing voltage versus different input voltage at 60 Hz by connecting the power line to a household 115-V 60-Hz electric outlet in an open-loaded state with resistance divider.

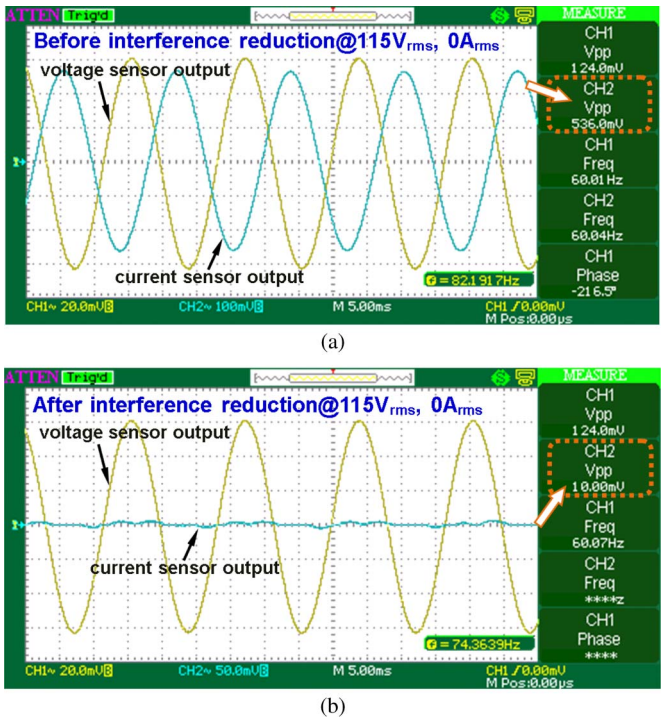


Fig. 11. Waveforms of the current sensor by sensing the power cord loaded with household 115-V 60-Hz supply before and after interference reduction.

sensing electrodes in an area of $1.3 \times 1$ cm$^2$, the sensor tag via the reading circuit exhibits a sensitivity of 271.6 mV/A and 0.38 mV/V for detecting 60-Hz electric current and voltage, respectively.

### *B. Interference Reduction for Current Measurement of Loaded Household Appliances*

For monitoring the household appliances using the sensor tag, the interference issue will be critical and observed during the current measurement of the power cord loaded with the input of 115 $V_{rms}$ 60 Hz. Fig. 11(a) shows the output waveforms of the current sensor attached to a household appliance

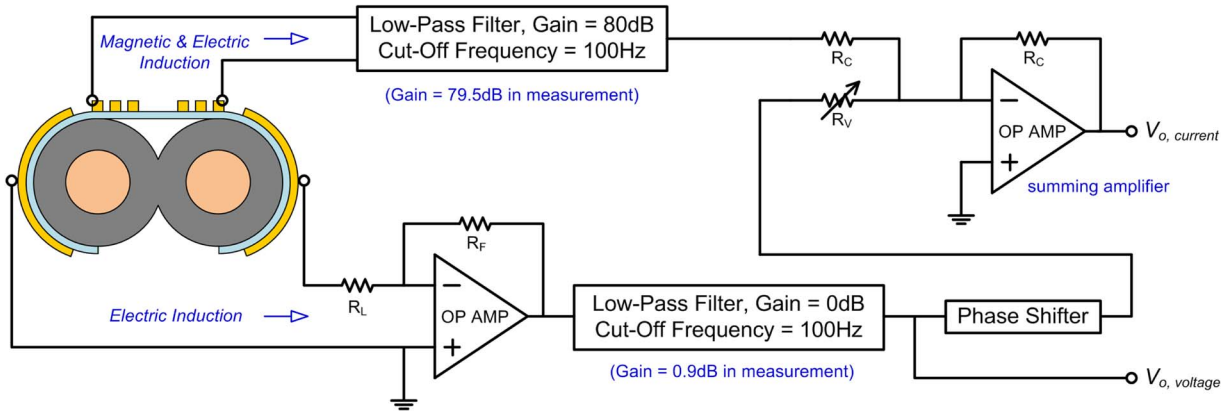


Fig. 12. Full circuit diagram for the noise elimination method.

where the power cord is plugged into the receptacle but not loaded with any current. The observed signal of the appliance in an OFF state mainly comes from the electric interference resulting from the time-variant electric field surrounding the fire line. Similar to the aforementioned sensing mechanism of the voltage sensor, the capacitive coupling effect will also cause an ac current flowing in the current sensor coil. Therefore, both inductive and capacitive coupled signals will be induced simultaneously in the sensor coil with the same frequency. A similar phenomenon has been found in the current sensor coil encircling a single power wire for the power sensing of industry electronics [20]. In fact, several research works have proposed employing a physical grounded metal shield for suppressing the electric interference [8], [28]. Instead of increasing the process complexity by adding the shielding structure, another interference reduction method combined with the voltage sensor is proposed to solve this problem as follows: Fig. 12 shows the full diagram of the current sensor readout circuit. Before the household appliance is turned on, the output signal of the voltage sensor is connected to a phase shifter to make the signal with 180° phase shift with respect to the initial output signal of the current sensor and then connected to a summing amplifier for the interference reduction of the current sensor by controlling the ratio of $R_V/R_C$. Fig. 12(b) shows the output signal of the current sensor after the interference reduction, and the sensor can have an ∼41-dB signal-to-noise ratio while it is used for detecting the loaded current of 1 $A_{rms}$, 60 Hz on the power line. With the interference reduction scheme, the sensor tag can be widely used for measuring the power cord biased with high voltage inputs. In this paper, the power sensor tag is utilized for monitoring the electricity of a hair dryer electric fan for the demonstration of the sensor tag for the power detection of household appliances. Fig 13 shows the measurement results. The detected current sensor signal of 1.76 $V_{pp}$, corresponding to a current input of 2.29 $A_{rms}$, is almost the same as the one measured by the current meter. Less than 1% inaccuracy can be accomplished. For further application, automatic calibration designed with digital electronic circuits is underway.

Inductive and capacitive coupling structures are two main sensor bodies in the power sensor. For the capacitive-type coupling, the capacitance between the sensing electrode and the inner conductor of the fire line is about 1 pH. The noise $V_{TC}$

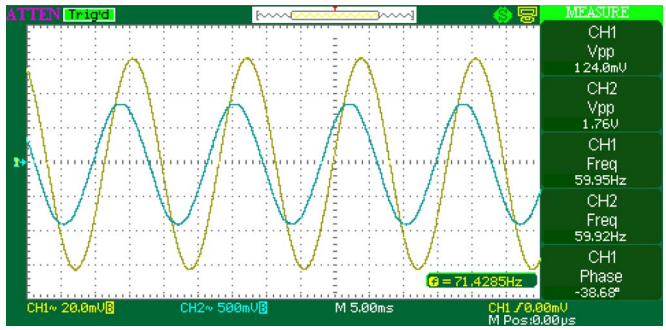


Fig. 13. Waveforms of the current and voltage sensor by sensing a 0.28-$A_{rms}$ 60-Hz electric current from the household 115-$V_{rms}$ 60-Hz power supply, respectively.

resulting from the capacitance and the series resistance of the sensor can be calculated as follows [29]:

$$V_{TC} = \sqrt{k_B \cdot T/C} \tag{8}$$

where $k_B$ is the Boltzmann constant, $1.38 \bullet 10^{-23}$ J/K, and $T$ is the working temperature of the sensor. It is $\sim 4\ \mu$V that is at least two orders of magnitude smaller than the detected signal. Meanwhile, for the current sensor part, the thermal noise $V_{TI}$ for the inductive coil can be calculated as follows:

$$V_{TI} = 2\sqrt{k_B \cdot T \cdot \Delta f \cdot R} \tag{9}$$

where $R$ is the coil resistance and $\Delta f$ is the frequency bandwidth [30]. In this case, the inductance and resistance of the sensor coil are about a submillihertz (0.5 mH) and hundreds of ohms (600 Ω), respectively. The noise is therefore about several tens of nanovolts for a bandwidth of 10 kHz, which is also three orders of magnitude smaller than the detected signal. From the calculation, the noise level is much smaller than the signal to be detected, so the sensor will not be susceptible to ambient temperature variability. Nevertheless, for future applications, the noise issue should be considered in the customized IC design for the sensor operation since the equivalent noise of these reactance components strongly depends on sensor interface circuits.

Table I summarizes the main features of the proposed current sensor and representative prior arts. This work compares

TABLE I
COMPARATIVE RESULTS WITH STATE-OF-THE-ART CURRENT SENSORS FOR LOW-FREQUENCY MEASUREMENTS

| *Comparison* | Leland *et al.* 2010 [13] | Schulz *et al.* 2010 [31] | Chen *et al.* 2012 [32] | Ouyang *et al.* 2012 [33] | *This work* |
|---|---|---|---|---|---|
| *Current Sensor Type* | Piezoelectric | Rogowski coil | Optic/Faraday rotation | GMR | *Faraday's law of induction* |
| *Current Sensor Size* | 1mm*0.2mm | 9mm*9mm | N. A. | > 10mm*10mm | *10mm*5mm* |
| *Sensor Output* | 1.08mV/A@60Hz | 265mV/A@50Hz | 4.4μrad/A@30Hz | 28mV/A@50Hz | *271.6mV/A@ 60Hz* |
| *Circuit Gain* | 40dB | 100dB | N. A. | N. A. | *80dB* |
| *Household Two-Wired Application* | Yes | No | No | No | *Yes* |
| *Manufacturing/Cost* | Complicated/Potential to be low | Simple/Low | Complicated/Potential to be low | Simple/Low | Simple/Low |
| *Susceptible to DC magnetic field* | N.A. | No | No | Possible | *No* |

*N.A. represents "Not Available"

favorably in small form factor and low cost and is nonintrusive by design. Additionally, it provides voltage sensing in the same package. Therefore, the proposed sensor tag has great promise for electricity monitoring of household appliances.

## IV. CONCLUSION

The electricity monitoring of household appliances using a flexible power sensor tag with an interference reduction scheme has been successfully demonstrated. The tag comprises current and voltage sensors operated by Faraday's induction law and capacitive coupling principle, respectively, and fabricated on the same flexible PET substrate using a flexible wafer-level chip-scale fabrication process. The characteristics of lower manufacturing cost, better reliability, and easier implementation have shown the potential of the flexible nonintrusive power sensor tag for widespread power detection of household appliances.

## ACKNOWLEDGMENT

The authors would like to thank the Nano Facility Center in National Chiao Tung University for the support of the fabrication facility and the National Center for High-Performance Computing for the support of the electromagnetic simulator.

## REFERENCES

[1] J. Scheffran and A. Battaglini, "Climate and conflicts: The security risks of global warming," *Reg. Environ. Change*, vol. 11, no. 1, pp. 27–39, Mar. 2011.
[2] E. A. Arens, D. Auslander, D. Culler, C. Federspiel, C. Huizenga, J. Rabaey, P. Wright, and D. White, Demand Response Enabling Technology Development, Phase I Report, Berkeley, CA, USA. [Online]. Available: http://www.escholarship.org/uc/item/0971h43j
[3] P. Ripka, "Electric current sensor: A review," *Meas. Sci. Technol.*, vol. 21, no. 11, pp. 112001-1–112001-23, Nov. 2010.
[4] S. Ziegler, R. C. Woodward, H. H. Iu, and L. J. Borle, "Electric current sensors: A review," *IEEE Sensors J.*, vol. 9, no. 4, pp. 354–376, Apr. 2009.
[5] C. Xiao, "An overview of integratable current sensor technologies," in *Conf. Rec. IEEE 38th IAS Annu. Meeting*, Salt Lake City, UT, USA, Oct. 2003, vol. 2, pp. 1251–1258.
[6] A. Radun, "An alternative low-cost current-sensing scheme for high-current power electronics circuits," *IEEE Trans. Ind. Electron.*, vol. 42, no. 1, pp. 78–84, Feb. 1995.
[7] E. Abdi-Jalebi and R. McMahon, "High-performance low-cost Rogowski transducers and accompanying circuitry," *IEEE Trans. Instrum. Meas.*, vol. 56, no. 3, pp. 753–759, Jun. 2007.
[8] M. Rigoni, J. S. D. Garcia, A. P. Garcia, P. A. Da Silva, N. J. Batistela, and P. Kuo-Peng, "Rogowski coil current meters," *IEEE Potentials*, vol. 27, no. 4, pp. 40–45, Jul./Aug. 2008.
[9] P. Poulichet, F. Costa, and E. Laboure, "A new high-current large-bandwidth dc active current probe for power electronics measurements," *IEEE Trans. Ind. Electron.*, vol. 52, no. 1, pp. 243–254, Feb. 2005.
[10] T. M. Liakopoulos and C. H. Ahn, "A micro-fluxgate magnetic sensor using micromachined planar solenoid coils," *Sens. Actuators A, Phys.*, vol. 77, no. 1, pp. 66–72, Sep. 1999.
[11] L. Rovati and S. Cattini, "Zero-field readout electronics for planar fluxgate sensors without compensation coil," *IEEE Trans. Ind. Electron.*, vol. 59, no. 1, pp. 571–578, Jan. 2012.
[12] N. A. Stutzke, S. E. Russek, D. P. Pappas, and M. Tondra, "Low-frequency noise measurements on commercial magnetoresistive magnetic field sensors," *J. Appl. Phys.*, vol. 97, no. 10, pp. 10Q107-1–10Q107-3, May 2005.
[13] V. Frick, L. Hébrard, P. Poure, F. Anstotz, and F. Braun, "CMOS microsystem for ac current measurement with galvanic isolation," *IEEE Sensors J.*, vol. 3, no. 6, pp. 752–760, Dec. 2003.
[14] E. S. Leland, P. K. Wright, and R. M. White, "A MEMS ac current sensor for residential and commercial electricity end-use monitoring," *J. Micromech. Microeng.*, vol. 19, no. 9, pp. 094018-1–094018-6, Sep. 2009.
[15] E. S. Leland, C. T. Sherman, P. Minor, R. M. White, and P. K. Wright, "A new MEMS sensor for ac electric current," in *Proc. IEEE Sensors*, Waikoloa, HI, USA, Nov. 2010, pp. 1177–1182.
[16] G. Wijeweera, B. Bahreyni, C. Shafai, A. Rajapakse, and D. R. Swatek, "Micromachined electric-field sensor to measure ac and dc fields in power systems," *IEEE Trans. Power Del.*, vol. 24, no. 3, pp. 988–995, Jul. 2009.
[17] C. Li and X. Cui, "An optical voltage and current sensor with electrically switchable quarter waveplate," *Sens. Actuators A, Phys.*, vol. 126, no. 1, pp. 62–67, Jan. 2006.
[18] A. Rowe, M. Berges, and R. Rajkumar, "Contactless sensing of appliance state transitions through variations in electromagnetic fields," in *Proc. ACM BuildSys.*, Zurich, Switzerland, Nov. 2010, pp. 19–24.
[19] M. A. Noras, "Solid state electric field sensor," in *Proc. ESA Annu. Meet. Electrostat.*, Cleveland, OH, USA, Jun. 2011, pp. 1–6.
[20] T. Kubo, T. Furukawa, H. Fukumoto, and M. Ohchi, "Numerical estimation of characteristics of voltage–current sensor of resin molded type for 22 kV power distribution systems," in *Proc. ICCAS-SICE*, Fukuoka, Saga, Japan, Aug. 2009, pp. 5050–5054.
[21] Y. C. Chen, W. H. Hsu, S. H. Cheng, and Y. T. Cheng, "A flexible, non-intrusive power sensor tag for the electricity monitoring of two-wire household appliances," in *Proc. IEEE Int. Conf. MEMS*, Paris, France, Jan. 2012, pp. 620–623.
[22] D. K. Cheng, *Field and Wave Electromagnetics,* 2nd ed. Reading, MA, USA: Addison-Wesley, 1989.
[23] Y. C. Chen, S. C. Yu, S. H. Cheng, and Y. T. Cheng, "A flexible inductive coil tag for household two-wire current sensing applications," *IEEE Sensors J.*, vol. 12, no. 6, pp. 2129–2134, Jun. 2012.
[24] V. Leus and D. Elata, "Fringing field effect in electrostatic actuators," Technion—Israel Inst. Technol., Haifa, Israel, Tech. Rep. ETR 2004-2, 2004.
[25] T.-Y. Chao, C.-W. Liang, Y.-T. Cheng, and C.-N. Kuo, "Heterogeneous chip integration process for flexible wireless microsystem application," *IEEE Trans. Electron Devices*, vol. 58, no. 3, pp. 906–909, Mar. 2011.

[26] F. S. Shieu, C. F. Chen, J. G. Sheen, and Z. C. Chang, "Intermetallic phase formation and shear strength of a Au-In microjoint," *Thin Solid Films*, vol. 346, no. 1/2, pp. 125–129, Jun. 1999.
[27] Texas Instruments, FilterProTM. [Online]. Available: http://www.ti.com/tool/filterpro
[28] I. A. Metwally, "Self-integrating Rogowski coil for high-impulse current measurement," *IEEE Trans. Instrum. Meas.*, vol. 59, no. 2, pp. 353–360, Feb. 2010.
[29] J. Li and S. M. R. Hasan, "Design and performance analysis of a 866-MHz low-power optimized CMOS LNA for UHF RFID," *IEEE Trans. Ind. Electron.*, vol. 60, no. 5, pp. 1840–1849, May 2013.
[30] G. Q. Wu, D. H. Xu, B. Xiong, and Y. L. Wang, "A micromachined square extensional mode resonant magnetometer with directly voltage output," in *Proc. IEEE Int. Conf. MEMS*, Paris, France, Jan. 20–24, 2013, pp. 633–636.
[31] C. A. Schulz, S. Duchesne, D. Roger, and J.-N. Vincent, "Short circuit current measurements between transformer sheets," *IEEE Trans. Magn.*, vol. 46, no. 2, pp. 536–539, Feb. 2010.
[32] G. Y. Chen, T. Lee, R. Ismaeel, G. Brambilla, and T. P. Newson, "Resonantly enhanced Faraday rotation in an microcoil current sensor," *IEEE Photon. Technol. Lett.*, vol. 24, no. 10, pp. 860–862, May 2012.
[33] Y. Ouyang, J. He, J. Hu, and S. X. Wang, "A current sensor based on the giant magnetoresistance effect: Design and potential smart grid applications," *Sensors*, vol. 12, no. 11, pp. 15 520–15 541, Nov. 2012.

**Yung-Chang Chen** was born in Taiwan. He received the B.S. degree in electrical engineering from National Taiwan Ocean University, Keelung, Taiwan, in 2006 and the M.S. degree in electronics engineering from National Chiao Tung University, Hsinchu, Taiwan, in 2008, where he is currently working toward the Ph.D. degree in the Microsystems Integration Laboratory, Department of Electronics Engineering and the Institute of Electronics.

His current research focuses on the microelectromechanical-systems acoustic device for hearing aid applications and electric sensors for household two-wire applications.

**Wei-Hung Hsu** was born in Taipei, Taiwan, in 1988. He received the B.S. degree in physics from National Chung Cheng University, Chiayi, Taiwan, in 2010 and the M.S. degree in electronics engineering from National Chiao Tung University, Hsinchu, Taiwan, in 2012. His thesis focused on the development of the power sensor for household two-wire applications.

He is currently a research staff member with the Green Energy and Environment Research Laboratories, Industrial Technology Research Institute, Chutung, Taiwan.

**Shih-Hsien Cheng** was born in Chiayi, Taiwan, in 1975. He received the B.S. degree in control engineering from Feng Chia University, Taichung, Taiwan, in 1998 and the M.S. degree in electrical engineering from National Sun Yat-Sen University, Kaohsiung, Taiwan, in 2000. He is currently working toward the Ph.D. degree in the Institute of Electrical Control Engineering, National Chiao Tung University, Hsinchu, Taiwan.

He is also a research staff member with the Green Energy and Environment Research Laboratories, Industrial Technology Research Institute, Chutung, Taiwan. His current research interests include power electronics circuit and system design, neural networks, fuzzy theory, and wireless sensor network.

**Yu Ting Cheng** (SM'07) was born in Taiwan, China. He received the B.S. and M.S. degrees in materials science and engineering from National Tsing Hua University, Hsinchu, Taiwan, in 1991 and 1993, respectively, the M.S. degree in materials science and engineering from Carnegie Mellon University, Pittsburgh, PA, USA, in 1996, and the Ph.D. degree in electrical engineering from the University of Michigan, Ann Arbor, MI, USA, in 2000. His Ph.D. thesis focused on the development of novel vacuum packaging technique for microelectromechanical systems (MEMS) applications.

He has been in Army service in Taiwan for two years. After finishing his Ph.D. study in 2000, he became a research staff member with the IBM Thomas J. Watson Research Center, Yorktown Heights, NY, USA, where he was involved in several system-on-a-package (SoP) projects. In 2002, he joined the Department of Electronics Engineering, National Chiao Tung University, Hsinchu, as an Assistant Professor and has been promoted as a Professor since 2009. His research interests include the fundamental study of materials for microsystem integration and nano/MEMS applications, SoP, and the design and fabrication of microsensors and microactuators.

Dr. Cheng was a corecipient of the 2006 Best Paper Award presented at the 13th IEEE International Conference on Electronics, Circuits and Systems. He has served as a Technical Program Committee member of IEEE NEMS since 2011, IEEE Sensors since 2012, IEEE Transducers 2013, IEEE ISMM 2012, and APCOT 2012. He is a member of the Institute of Physics and Phi Tau Phi.